

The NavINST Dataset for Multi-Sensor Autonomous Navigation

Paulo Ricardo Marques de Araujo[§], Eslam Mounier[§], Qamar Bader, Emma Dawson, Shaza I. Kaoud Abdelaziz, Ahmed Zekry, Mohamed Elhabiby and Aboelmagd Noureldin

Abstract—The Navigation and Instrumentation (NavINST) Laboratory has developed a comprehensive multisensory dataset from various road-test trajectories in urban environments, featuring diverse lighting conditions, including indoor garage scenarios with dense 3D maps. This dataset includes multiple commercial-grade IMUs and a high-end tactical-grade IMU. Additionally, it contains a wide array of perception-based sensors, such as a solid-state LiDAR—making it one of the first datasets to do so—a mechanical LiDAR, four electronically scanning RADARs, a monocular camera, and two stereo cameras. The dataset also includes forward speed measurements derived from the vehicle’s odometer, along with accurately post-processed high-end GNSS/IMU data, providing precise ground truth positioning and navigation information. The NavINST dataset is designed to support advanced research in high-precision positioning, navigation, mapping, computer vision, and multisensory fusion. It offers rich, multi-sensor data ideal for developing and validating robust algorithms for autonomous vehicles. Finally, it is fully integrated with the robot operating system (ROS), ensuring ease of use and accessibility for the research community. The complete dataset and development tools are available at navinst.github.io.

I. INTRODUCTION

The last decade has witnessed significant advancements in autonomous driving, robotics, and computer vision, transforming these fields with innovative applications. In particular, autonomous vehicles (AVs) technology has ushered in a new era of transportation, promising increased safety, efficiency, and convenience [1]. These advancements in AVs are fundamentally reliant on robust navigation systems capable of achieving higher levels of autonomy by operating seamlessly in diverse and dynamic environments while ensuring accuracy, reliability, and adaptability [2].

A major enabler of these research advances has been the publication of diverse datasets by research groups that provide high-quality standardized data that supports the development, testing, and benchmarking of innovative algorithms. Datasets

such as the widely renowned KITTI dataset [3] have become foundational resources for tasks such as odometry, object detection, and sensor fusion, supporting thousands of research works around the world, overcoming limitations related to data accessibility and system constraints. After KITTI, more datasets were published introducing diverse sensor configurations, research focuses and challenges. For instance, the Oxford RobotCar dataset [4] tackles large-scale challenges with over 1000 km of multi-sensory data, the Complex Urban dataset [5] focuses light detection and ranging (LiDAR) technology in complex urban settings, the Mulran dataset [6] focuses on structural place recognition, UrbanNav [7] focuses on global navigation satellite system (GNSS)-challenged environments such as in deep urban areas, and Boreas [8] addresses multi-season challenges.

An integral component of these impactful datasets is the accompanying scientific paper that provides a detailed description of the dataset. The scope of dataset papers extends beyond simply presenting raw data. Their innovation lies in the thoughtful design, utility, and comprehensive documentation they provide, as well as the lessons learned throughout the production of the dataset. These documents enable researchers to seamlessly utilize the data for algorithm development and testing while allowing the research community to replicate, adapt, and extend the work. This, in turn, facilitates the creation of new systems and datasets to bridge research gaps, enhancing data quality and availability to fulfill the growing variety of research needs.

In this line of work, we have developed the Navigation and Instrumentation (NavINST) dataset, exemplifying thoughtful dataset design by providing a comprehensive collection of multi-modal sensor data tailored for research in high-precision positioning, navigation, mapping, and multi-sensor fusion. Constructed using robot operating system (ROS), the dataset was collected in Kingston, ON, and Calgary, AB, Canada, spanning approximately 80 kilometers of diverse urban and environmental conditions. It features repeated trajectories under varied lighting, traffic, and urban scenarios, as well as challenging indoor environments, making it a versatile resource for researchers, industry professionals, and developers in autonomous systems and navigation. The platform, illustrated in Fig. 1, integrates a comprehensive sensor suite and a robust reference system, detailed in more detail in section III. This platform will be used to continue to perform road tests in various environments and in different cities. We will continue to update the published data with the newly collected data to support research activities in the area.

[§] Authors contributed equally.

Paulo Ricardo Marques de Araujo, Qamar Bader, Emma Dawson, Ahmed Zekry, and Shaza I. Kaoud Abdelaziz were with the Department of Electrical and Computer Engineering, Queen’s University, Kingston, ON, Canada (e-mail: {paulo.araujo, qamar.bader, emma.dawson, ahmed.zekry, shaza.kaoud}@queensu.ca).

Eslam Mounier was with the Department of Electrical and Computer Engineering, Queen’s University, Kingston, ON, Canada, and the Ain Shams University, Cairo, Egypt (e-mail: eslam.abdelmoneem@queensu.ca).

Mohamed Elhabiby was with Micro Engineering Tech. Inc., Calgary, AB, Canada (email: elhabiby@microengineering.ca).

Aboelmagd Noureldin was with the Department of Electrical and Computer Engineering, Royal Military College of Canada, Kingston, ON, Canada (email: aboelmagd.noureldin@rmc.ca).

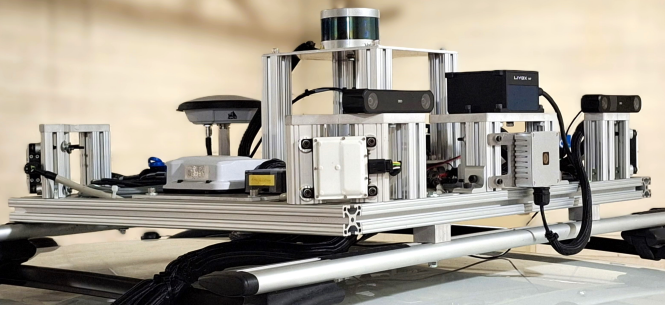


Fig. 1: NavINST multisensory platform.

The main contributions of the NavINST dataset are as follows:

- We repeated trajectories under different lighting conditions and across diverse urban scenarios.
- We collected data in two indoor garages, and we also provided the 3D maps of these environments.
- Our dataset includes data from multiple commercial inertial measurement units (IMUs), useful for advanced navigation-based research.
- Our dataset features a solid-state LiDAR, making it one of the first datasets to provide such data.
- The dataset features multiple radio detection and rangings (RADARs), including four electronically scanning RADARs (ESRs) providing 360° coverage around the vehicle, and a Doppler RADAR mounted on the bumper for forward speed estimation.
- We post-processed the GNSS/IMU data to provide accurate ground truth pose information for our outdoor trajectories.
- Our dataset is fully integrated with ROS ensuring convenient accessibility and usability, but a toolkit is also provided for those working offline.

The paper is structured as follows: Section II presents a literature survey of the existing positioning datasets. Section III presents the multisensory platform outlining the details of the sensor suite, including a description of the software architecture, reference system, and calibration. Section IV explains important information about data collection, and section V describes how the dataset is structured. Section VI presents some tests and demonstrations performed with the dataset, and section VII concludes the paper.

II. RELATED WORKS

Several datasets have been published in recent years to enable research in positioning and navigation through the fusion of perception sensors, onboard motion sensors, and GNSS. TABLE I summarizes a collection of these datasets.

One of the earliest contributions to this body of work is the KITTI odometry dataset [3]. It consists of data from four monocular cameras, a 64-channel LiDAR, as well as inertial and GNSS data. Additionally, all data is collected during daylight hours. More recent contributions to open navigation datasets include the Oxford RobotCar [4] and UrbanNav [7] datasets. Both provide camera, LiDAR and

inertial measurement data. The Oxford RobotCar explores nighttime (darkened) driving, and UrbanNav provides ROS support to users. Neither dataset includes RADAR data. The Complex Urban [5] dataset provides neither RADAR nor camera data but is interesting in that it provides both tactical and commercial grade IMU data and offers ROS support to facilitate its use.

RADAR technology has improved in the past decade, making it a promising sensor for positioning and navigation applications. As such, only a subset of existing datasets offer RADAR data within their sensor suite. The datasets including RADAR data are divided by the RADAR technology used: mechanically scanning RADAR or electronically scanning RADAR. The Oxford Radar [9], MulRan [6], and Boreas [8] datasets provide data from a mechanically scanning 360° RADAR. The data provided by these RADARs is high resolution, but the sensors are costly and do not provide Doppler velocity information [13]. Other datasets employ ESR instead. A 3D ESR provides range, azimuth, and Doppler velocity measurements for target objects. A 4D ESR provides an additional elevation angle measurement. MSC-RAD4R [10] and K-Radar [11] are interesting datasets, each providing data from a single 4D RADAR. However, 4D RADARs have limited fields of view, and a single RADAR cannot provide a 360° view of the vehicle's surroundings. The NavINST multisensory platform has four 4D ESR, enabling a 360° view of the vehicle's environment and providing Doppler velocity information for all targets.

The PixSet dataset published by Leddar Tech is among the first to provide data from a proprietary solid-state LiDAR alongside a 64-channel scanning LiDAR [12]. However, a single 3D RADAR mounted at the front bumper of the data collection vehicle provides limited opportunities for RADAR-based positioning research. Inertial data is restricted to a single tactical grade IMU. The NavINST dataset also provides a solid-state LiDAR and a 16-channel mechanical LiDAR, with the advantage of four 4D ESR for comparison and fusion opportunities.

III. NAVINST MULTISENSORY PLATFORM

In this section, we present the multisensory platform and its sensors, the ROS network, and the time synchronization strategy used to synchronize the multiple computers available in the vehicle. Also, we detail the post-processing approach to achieve accurate ground truth information and the intrinsic and extrinsic calibration of the perception sensors.

A. Sensors

The physical platform is shown in Fig. 1, and the coordinate systems of the sensors are presented in Fig. 2. The system is installed as a single unit on the vehicle's roof. This arrangement facilitates logistics and reduces the uncertainty of the extrinsic calibration. The data is stored in ROS *bag* files, in which each sensor data is stored under a specific topic name. Sometimes, a sensor provides more than one piece of information, which demands multiple message types. Such message types can be found in the dataset repository as

TABLE I: Related Positioning Datasets. MC: Monocular Camera. SC: Stereo Camera. SS: Solid-state LiDAR. A: Automotive 4D RADAR. N: 360° Navtech radar. T: Tactical-grade IMU. C: Commercial-grade IMU. GT: Ground truth pose source. RTK (Real-Time Kinematic) uses a GNSS base station and differential measurements to improve the estimations. RTX uses data from a global network of tracking stations to calculate corrections.

Name	Camera	LiDAR	RADAR	IMU	GT	Indoor	Night	ROS Support
KITTI (odometry) [3]	4× MC	1× 64 ch	×	1× T	GNSS/IMU + RTK	×	×	×
Oxford RobotCar [4]	1× SC + 3× MC	1× 4 ch + 2× 1 ch	×	1× T	GNSS/IMU	×	✓	×
Oxford Radar RobotCar [9]	1× SC + 3× MC	2× 32 ch + 2× 1 ch	1× N	1× T	GNSS/IMU + VO	×	×	×
UrbanNav [7]	1× SC	1× 32 ch + 2× 16 ch	×	1× C	GNSS/IMU + RTK	!	✓	✓
Complex Urban [5]	×	2× 16 ch + 2× 1 ch	×	1× T + 1× C	GNSS/IMU	!	×	✓
MSC-RAD4R [10]	1× SC	1× 128 ch	1× A	1× C	GNSS + RTK	!	✓	✓
MulRan [6]	×	1× 64 ch	1× N	×	SLAM	×	×	✓
K-Radar [11]	4× SC	1× 128 ch + 1× 64 ch	1× A	2× C	GNSS + RTK*	×	✓	×
Boreas [8]	1× MC	1× 128 ch	1× N	1× T	GNSS/IMU + RTX	×	✓	×
PixSet [12]	4× MC	1× SS + 1× 64 ch	1× A	1× T	GNSS/IMU + RTK	×	✓	×
NavINST	2× SC + 1× MC	1× SS + 1× 16 ch	4× A + 1× 1D	4× C + 1× T	GNSS/IMU + RTK	✓	✓	✓

! tunnels in some of the trajectories. * no GT reference is mentioned in the paper, this may be the most accurate information available.

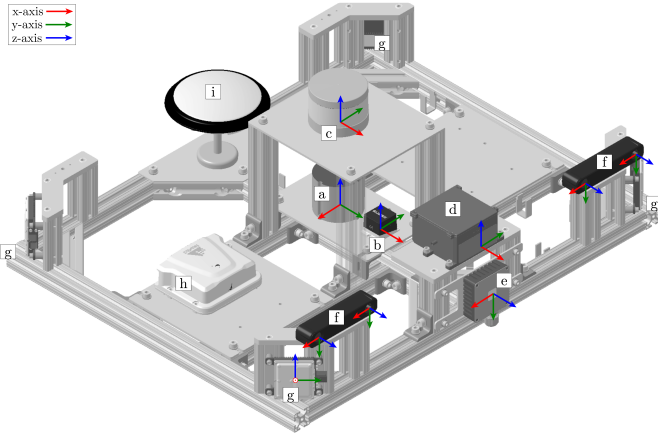


Fig. 2: Sensors and their coordinate systems.

detailed in section V. Specifications, topic names, and message types for sensors are summarized in TABLE II.

The platform was designed for 360° coverage, combining multiple sensors to achieve this objective, as shown in Fig. 3. The dataset includes cameras that are mounted in a configuration that can facilitate various investigations. For example, the multiple aligned cameras can be used to build different baselines for stereo vision applications.

Each stereo camera contains an IMU, but the manufacturer has not disclosed the model. Internal tests indicate that this IMU is of a commercial grade. Additionally, the solid-state LiDAR is equipped with a Bosch BMI088 IMU. Combined with the IMU inside the MTi-670G, the dataset includes four commercial IMUs, providing ample opportunities for various investigations. In addition, our dataset includes two GNSS receivers, the Novatel PwrPak7-E1 and the Xsens MTi-670G, which can be used to investigate different fusion algorithms with both high-end and commercial-grade receivers.

Another important addition to the dataset is the set of sensors capable of generating point clouds, which can be used for map registration and simultaneous localization and mapping (SLAM). The four RADARs are hardware synchronized, thus generating a unified point cloud with 360° coverage, as shown in Fig. 4a. The point clouds generated by the VLP-16 LiDAR and the Livox HAP LiDAR are illustrated in Fig. 4b and

Fig. 4c, respectively.

Finally, the dataset includes a 1D Doppler RADAR mounted on the vehicle’s bumper, as presented in Fig. 5. The sensor is mounted facing the ground at an angle and can only provide the Doppler speed of a single detection. As discussed in section VI-G, it can be used with an intelligent system to estimate the vehicle’s forward speed.

B. Data Collection Framework

The sensors mentioned above are connected to two computing systems responsible for synchronized data recording: a main computer (13th Gen Core i7, 32G DDR5 RAM, 1TB SSD) and a secondary computer, the NVIDIA Orin™ NX (8-core Arm Cortex, 16 GB LPDDR5 RAM, 1TB SSD). The overall system architecture, including the various sensor connections, is illustrated in Fig. 6. A range of connection types were employed to accommodate the diverse sensor systems. Some sensors were connected to the main computer via Ethernet-based connectivity through Ethernet switch-1. Other sensors utilize universal serial bus (USB) connectivity through dedicated ports on the main computer. The Stereolabs ZED X cameras, which require high bandwidth, were connected directly to the secondary computer using a gigabit multimedia serial link (GMSL). The main and secondary computers are interconnected via Ethernet switch-2, establishing a unified and integrated system.

Given the complexity of the system and the need for a unified time reference across multiple sensor data, time synchronization is deemed essential. To that end, we adopted the ROS, a robust solution widely used for managing synchronization across multiple devices in the robotics domain [14]. Both computers run Linux with ROS installed. A ROS network was established with the main computer acting as the ROS master, coordinating communication across the different ROS nodes. Each computer independently records data from its connected sensors, with ROS ensuring that all sensor messages are synchronized with the UNIX time of the respective computer.

We employed ROS software drivers provided by sensor manufacturers or third parties to operate each sensor and obtain data. These drivers were modified and, in some cases, developed to meet our specific requirements. Our system employed ROS1 and ROS2 environments simultaneously, ne-

TABLE II: Specifications, ROS topic names, and message types for sensors.

Label	Sensor	Specifications	Qty	Hz	Topic Name	Message Type
a	KVH1750 IMU	Gyroscope - Bias stability: $0.05^\circ/\text{h}$ - Noise density: $0.012^\circ/\sqrt{\text{h}}$ Accelerometer - Bias stability: 7.5 mg - Noise density: $0.0701 \text{ m/s}/\sqrt{\text{h}}$	1	200	/novatel/imu	sensor_msgs/Imu
b	Xsens MTi-670G IMU/GNSS	Gyroscope - In-run bias stability: $8^\circ/\text{h}$ - Noise density: $0.007^\circ/\text{s}/\sqrt{\text{Hz}}$ Accelerometer - In-run bias stability: 10 (x,y) 15 (z) μg - Noise density: $60 \mu\text{g}/\sqrt{\text{Hz}}$ GNSS receiver - u-blox ZED F9	1	100	/xsens/imu /xsens/gnss /xsens/mag /xsens/pressure /xsens/temperature /xsens/filter/quaternion /xsens/filter/positionlla /xsens/filter/twist	sensor_msgs/Imu sensor_msgs/NavSatFix geometry_msgs/Vector3Stamped sensor_msgs/FluidPressure sensor_msgs/Temperature geometry_msgs/QuaternionStamped geometry_msgs/Vector3Stamped geometry_msgs/TwistStamped
c	Velodyne VLP-16 3D Mechanical LiDAR	HFOV: 360° VFOV: 30° Angular resolution - H: $0.1^\circ - 0.4^\circ$ - V: 2.0°	1	10	/velodyne/lidar/points	sensor_msgs/PointCloud2
d	Livox HAP 3D Solid-state LiDAR	HFOV: 120° VFOV: 25° Angular resolution - H: 0.18° - V: 0.23°	1	10	/livox/lidar/points /livox/lidar/imu	sensor_msgs/PointCloud2 sensor_msgs/Imu
e	Luxonis OAK-1 W PoE Monocular Camera	DFOV: 150° HFOV: 127° VFOV: 79.5° Resolution: 1MP (1280×720) Shutter: Global	1	30	/oak/camera_info /oak/image_raw_color/compressed	sensor_msgs/CameraInfo sensor_msgs/CompressedImage
f	Stereolabs ZED X Stereo Camera	DFOV: 120° HFOV: 110° VFOV: 80° Resolution: 1MP (960×540) Shutter: Global Baseline: 120 mm	2	15	/zedx_left/imu /zedx_left/temperature /zedx_left/camera_left/camera_info /zedx_left/camera_left/image_raw_color/compressed /zedx_left/camera_right/camera_info /zedx_left/camera_right/image_raw_color/compressed /zedx_right/imu /zedx_right/temperature /zedx_right/camera_left/camera_info /zedx_right/camera_left/image_raw_color/compressed /zedx_right/camera_right/camera_info /zedx_right/camera_right/image_raw_color/compressed	sensor_msgs/Imu sensor_msgs/Temperature sensor_msgs/CameraInfo sensor_msgs/CompressedImage sensor_msgs/CameraInfo sensor_msgs/CompressedImage sensor_msgs/Imu sensor_msgs/Temperature sensor_msgs/CameraInfo sensor_msgs/CompressedImage sensor_msgs/CameraInfo sensor_msgs/CompressedImage
g	Smartmicro UMRR-96 Type 153 4D ESR	Range: 0.15 m ... 19.3 m Range accuracy: $<0.15 \text{ m}$ Speed: $-400 \dots 140 \text{ km/h}$ Speed accuracy: $<0.15 \text{ m/s}$ HFOV: 130° VFOV: 15° Horizontal accuracy: $\leq 1^\circ$ Vertical accuracy: $\leq 2^\circ$	4	20	/smartmicro/radar/front_left /smartmicro/radar/front_right /smartmicro/radar/rear_left /smartmicro/radar/rear_right	sensor_msgs/PointCloud2
h	Novatel PwrPak7-E1 GNSS/IMU	Constellations: GPS, GLONASS, BeiDou, Galileo, IRNSS, SBAS, QZSS, NavIC Single point accuracy: 1.5 m SBAS accuracy: 0.60 m RTK accuracy: 0.01 m + 1 ppm IMU: EPSON G320N - Gyro Input Range: $\pm 150^\circ/\text{s}$ - Bias Repeatability: $0.5^\circ/\text{s}$ - Angular Random Walk: $0.1^\circ/\sqrt{\text{h}}$ - Accelerometer Range: $\pm 5 \text{ g}$ - Accelerometer Bias Repeatability: 15 mg	1	50 125	/novatel/gps /novatel/Imu*	gps_common/GPSFix sensor_msgs/Imu
i	Novatel VEXXIS GNSS-850	GNSS Antenna	1	-	-	-
-	OBDII Automotive Scanner	FORS-CAN ELM327 - On-Board Diagnostics V2 Protocols - USB2.0	1	16	/obd2/speed /obd2/rpm /obd2/maf	<input type="checkbox"/>
-	OPS241-A 1D Doppler RADAR	Range: 1 m ... 25 m Maximum speed: 223 km/h Speed resolution: 0.436 km/h	1	20	/omnripresense/radar/front_bumper	<input type="checkbox"/>

☐ custom message. * available in indoor trajectories only.

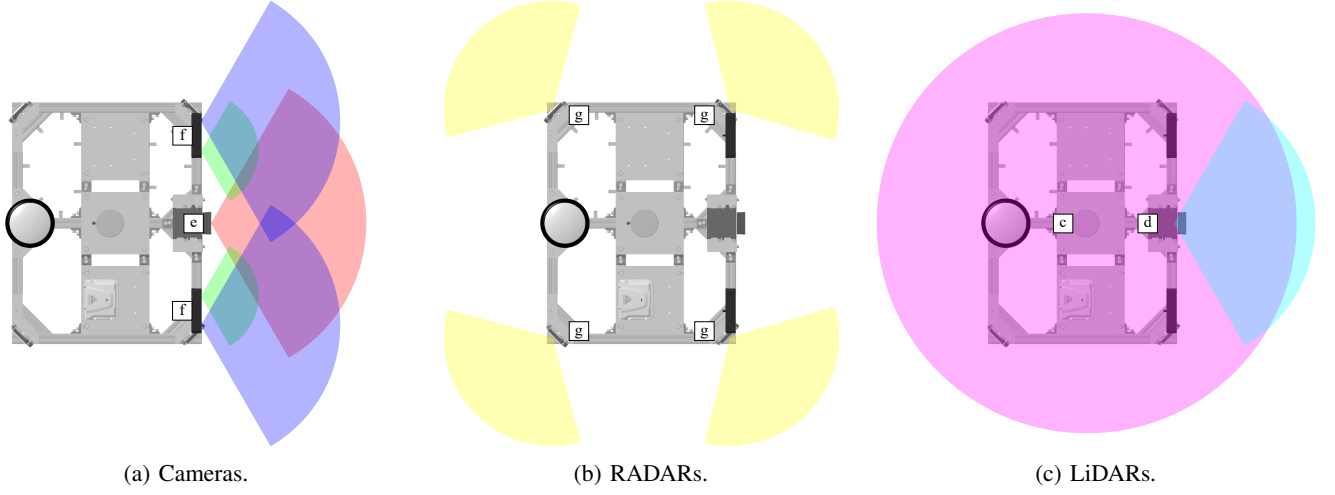


Fig. 3: Schematic representation of the field of view of perception sensors.

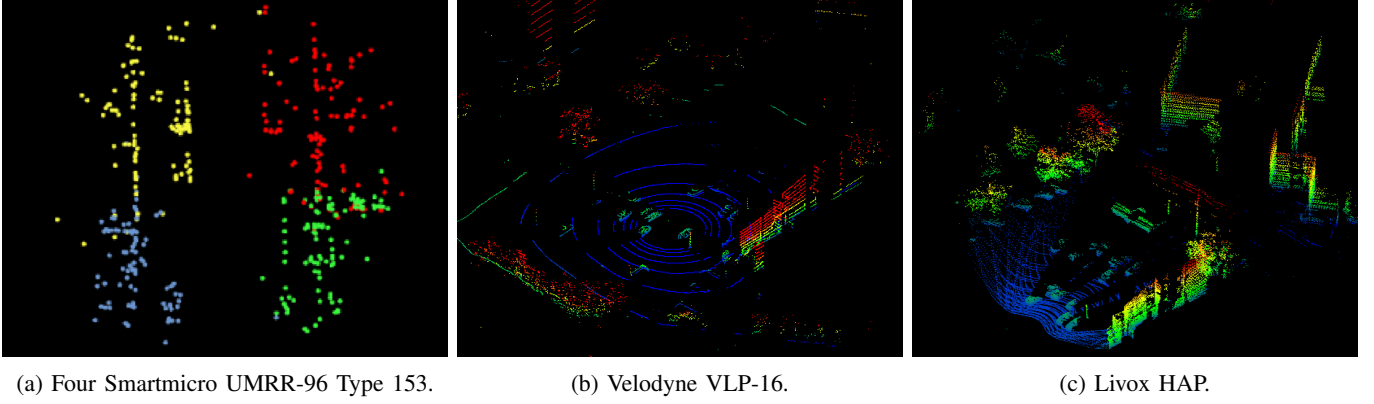


Fig. 4: Point cloud examples.



Fig. 5: Omnipresense OPS241-A mounted on the front bumper.

cessitating a bridge to convert ROS2 topics into ROS1 topics for a unified data recording process.

To streamline the data collection process, we developed a distributed software tool for synchronized sensor launch, monitoring, and data acquisition. This tool enabled a systematic launch of the necessary sensor drivers, conducting

essential tests to detect successful sensor operation, performing periodic checks to detect any communication failures, and locally recording timestamped data from the desired sensors.

While ROS ensures synchronization of sensor messages within each computer's UNIX timestamp, time drift can occur between multiple computers, which will cause different sensors recording on different computers to have a misaligned time frame. To address this, we utilized well-established time synchronization tools, such as *Chrony* and *GPSd* services, to create an efficient and transparent time synchronization background process [15]. *Chrony*, an effective network time protocol (NTP) implementation, was used to configure the main computer as the NTP server and the secondary computer as the NTP client, ensuring that the secondary computer's clock is continuously updated to match the server's time. Additionally, *GPSd* was used to monitor a dedicated M8T Ublox GNSS receiver, providing precise timing information. *Chrony* was configured to calibrate the main computer's time using the GNSS data, which was then propagated to the secondary computer, ensuring unified GNSS-aligned time synchronization across the entire ROS network.

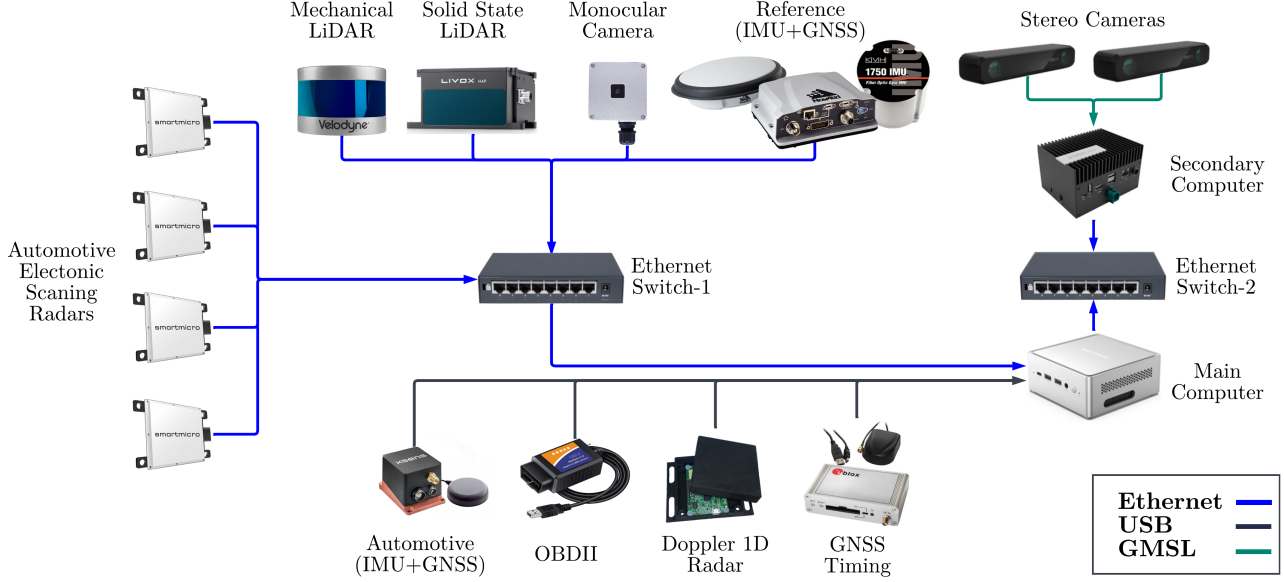


Fig. 6: The system's architecture including its components and connections.

C. Ground Truth

The reference positioning solution is achieved by employing Novatel's advanced PwrPak7-E1 GNSS receiver, which is seamlessly integrated with the high-end tactical-grade KVH1750 IMU. To augment the accuracy of the ground truth solutions, stationary antennas were used to conduct differential GNSS processing, commonly known as post-processed kinematic (PPK) [16]. Later, the reference solution is post-processed using Inertial Explorer by combining loosely-coupled integration with differential GNSS along with tightly-coupled integration.

Positions, namely, latitude, longitude, and altitude are given in the geodetic frame. Velocities are given with respect to a fixed east-north-up (ENU) frame. The attitude information, namely pitch, roll, and azimuth is given in degrees. Each trajectory includes 50 Hz ground truth data, with an extended version including statistics at 1 Hz. This post-processed information is injected into the *bag* files using ROS timestamps while keeping the GPS timestamps. Further details about the data format are presented in section V.

The standard deviations provided by Inertial Explorer exhibit variation dependent on factors such as satellite visibility (influenced by the environment and time of day), trajectory length, and vehicle dynamics. This information is also available in the *bag* files storing reference data. For position, the average standard deviations fall within the range of 1 centimeter, while for orientation, they are below 0.02° for trajectories Urban01 to Urban04. Fig. 7 illustrates a sample standard deviations extracted from a trajectory after being post-processed. For trajectories Urban05 and Urban06, due to the challenging GNSS environment, the position standard deviations fall within the range of 50 centimeters, while the orientation standard deviations fall within 0.58° for pitch and roll and 2.08° for heading in some areas.

In indoor environments, where GNSS signals are signifi-

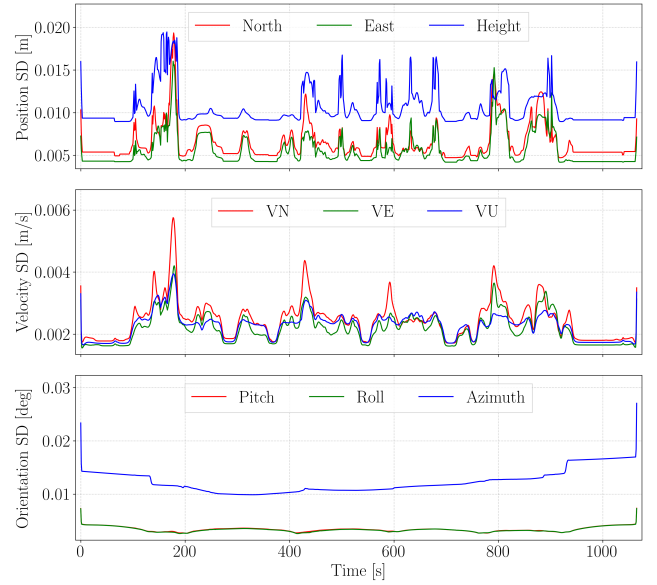


Fig. 7: Post-processed standard deviations of position, velocity, and orientation, as reported by Inertial Explorer to trajectory Urban04.

cantly degraded, our high-precision GNSS/IMU reference system becomes unreliable. As an alternative, we offer a different ground truth solution: the LiDAR-to-map registration (LMR) approach presented in [17]. This method integrates IMU and vehicle odometer measurements, periodically correcting the vehicle's pose using LiDAR measurements registered to available map data. The LMR approach employs an elaborate pipeline that utilizes an extended Kalman filter for sensor fusion and an optimized map filtering algorithm to improve the efficiency of point cloud registration. The LMR solution is provided in the local level frame of the map with Cartesian 3D position components in meters and attitude information,

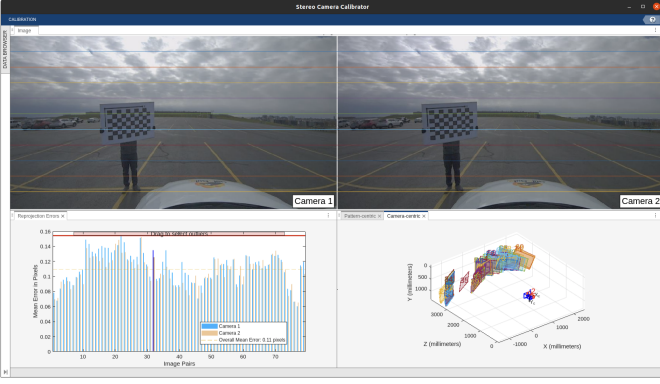


Fig. 8: Calibration of the ZED X (left) stereo camera inside MATLAB Stereo Camera Calibrator toolbox.

i.e., pitch, roll, and azimuth, in degrees, sampled at 50 Hz.

In urban environments, the LMR solution has demonstrated sub-meter accuracy, with a root mean square position error of 20 centimeters. Given this strong performance, it is reasonable to expect that this approach will achieve comparable, if not superior, positioning accuracy in indoor environments, particularly due to slower vehicle dynamics. This makes the LMR solution a reliable reference for comparison in challenging indoor settings. However, it is important to note that the accuracy of the LMR solution is highly dependent on the quality of the offline maps used.

D. Calibration

Since our platform includes multiple cameras, we provide some of the calibration parameters used in sections VI-D and VI-E. The cameras were calibrated using MATLAB’s camera calibrator and stereo camera calibrator toolboxes. To offer greater flexibility to researchers, we also include the *bag* file recorded for calibration, which contains stationary data. This data can be useful for calibrating additional sensors as needed. Fig. 8 illustrates the environment and calibration board used in this *bag* file.

We also provide the calibration between the OAK camera and the VLP-16 LiDAR. These sensors were calibrated using MATLAB’s LiDAR Camera Calibrator toolbox and the calibration *bag*. Fig. 9 shows an example of the estimated calibration parameters. In this example, a vehicle is detected using the MATLAB vehicle detector, and the bounding box of the detection is then projected onto the VLP-16 point cloud.

The reference system undergoes a calibration routine, following Novatel’s recommendations, to calculate the Body-to-Vehicle Frame Rotation, ensuring accurate kinematic alignment. This alignment has already been compensated for in the provided solutions. The remaining sensors were carefully assembled according to the 3D CAD system (Fig. 2), with all distances measured to an uncertainty of less than 1 centimeter. We also provide ROS launch files that include the transformation tree connecting all sensors.

IV. TRAJECTORIES

The dataset includes both outdoor and indoor trajectory data recorded in urban environments across Kingston, ON, and

TABLE III: Metadata of the trajectories. (D) for a daytime trajectory and (N) for a nighttime trajectory.

Trajectory		Length (km)	Duration (min)	Avg. Speed (km/h)	Max. Speed (km/h)
Urban01	(D)	8.70	35.42	14.75	47.11
Urban01	(N)	8.68	31.12	16.74	44.87
Urban02	(D)	6.78	23.58	17.26	40.49
Urban02	(N)	6.79	24.20	16.82	40.61
Urban03	(D)	5.21	21.53	14.51	43.05
Urban03	(N)	5.17	18.50	16.77	45.43
Urban04	(D)	4.87	17.75	16.46	44.57
Urban04	(N)	4.87	16.42	17.79	51.85
Urban05	(D)	9.77	34.25	17.12	44.49
Urban06	(D)	9.61	36.55	15.78	44.37
Indoor01		1.25	7.03	10.63	23.52
Indoor02		0.97	5.86	9.93	22.13
Indoor03		1.27	8.43	9.00	22.20
Indoor04		1.80	14.20	7.48	12.69
Indoor05		1.25	9.90	7.58	15.17
Total		76.99	304.74	-	-

Calgary, AB, in Canada. Kingston is primarily a residential area with abundant vegetation, while downtown Calgary is a dense urban setting with numerous high-rise buildings. These two environments present distinct challenges for autonomous vehicle navigation. Fig. 10 shows the six outdoor trajectories and their metadata is detailed in TABLE III.

All trajectories followed the same protocol. The reference system was initialized in an open-sky area. Next, all sensors were powered up to ensure that no biases accumulated during the initialization of the reference system. The main computer was then time-synchronized using the GNSS timing receiver. Subsequently, the secondary computer was synchronized to the main computer, and recording was initiated. The vehicle remained stationary at the beginning and end of the trajectories for approximately 2 minutes.

The outdoor trajectories were collected during both day and night to enable the investigation of computer vision-based methods for urban navigation under different lighting conditions, see Fig. 12. Therefore, eight outdoor trajectories are provided, totaling approximately 50 kilometers of recorded data.

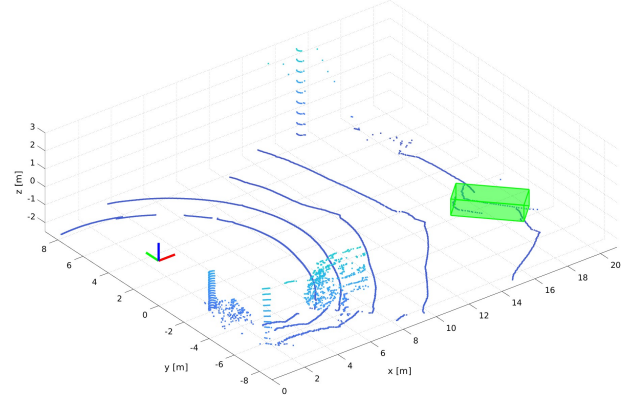
The dataset includes five indoor trajectories recorded in two indoor underground garages, as illustrated in Fig. 11. As shown in Fig. 12(c), the selected garages are confined spaces that pose multiple challenges for perception sensors. To further contribute to the community, we provide high-definition 3D maps of both garages, which were prepared using a high-definition stationary LiDAR. All trajectories started outside where GNSS was available for proper initialization of the respective reference system. After a few minutes, the vehicle was driven throughout the garage before returning outside to complete the recording.

V. DATASET ORGANIZATION

The dataset is organized as shown in Fig. 13. Both day and night outdoor trajectories are organized into folders named as Urban01...Urban06. Inside these subfolders named with a specific timestamp, one can find various *bag* files named according to their contents. For example, all camera-related data are stored in the *cameras.bag* file. We structured the *bag* files this way to facilitate their use; users



(a) MATLAB Vehicle detector using an OAK camera image.



(b) Image bounding box projection onto VLP-16 point cloud.

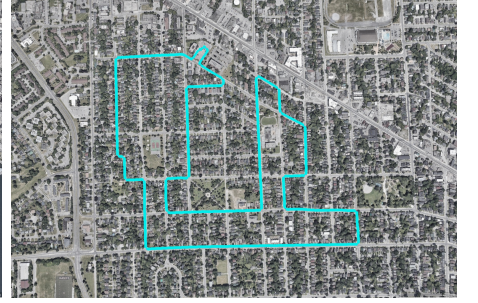
Fig. 9: Camera and LiDAR calibration example.



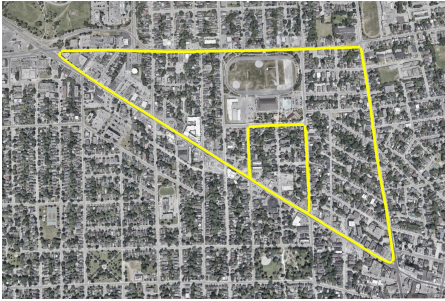
(a) Urban01.



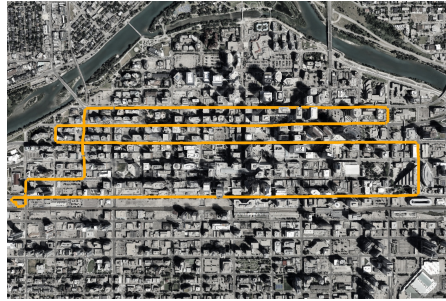
(b) Urban02.



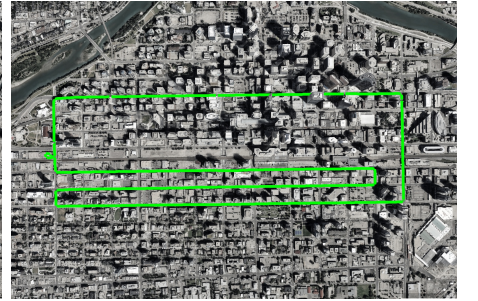
(c) Urban03.



(d) Urban04.



(e) Urban05.



(f) Urban06.

Fig. 10: Outdoor trajectories.

can download only the *bag* files of interest and play them together using the command `roslaunch play *`, assuming all *bag* files are stored in the same directory. In addition to the trajectory folders, the user can find the *IndoorMaps* folder, which contains the PCD format files of the indoor maps, and the *CalibrationData* folder, which includes the calibration files and MATLAB projects of the tools discussed in section III-D, the *bag* file recorded for calibration, the ROS launch file to launch the transformation tree and the transformations considering KVH1750 as the origin (see file `setup_transformation.txt`).

VI. DEMONSTRATIONS

To demonstrate our dataset's validity, we test various navigation and positioning algorithms. The objective of the demon-

strations is to validate the functionality of the data, rather than proposing, validating, or criticizing positioning methods.

A. Evaluation Metrics

To evaluate the performance of the tested systems while using the NavINST dataset, we use two error metrics:

- 1) absolute trajectory error (ATE): Measures the root-mean-square error between the predicted 3D pose and the ground truth to assess the global consistency of the estimated trajectory. We split the analysis into translational error (*trans*) expressed in meters and rotational error (*rot*) expressed in degrees.
- 2) relative pose error (RPE): Measures the error in the relative motion between consecutive poses, which helps in assessing the drift in the estimated trajectory. It is

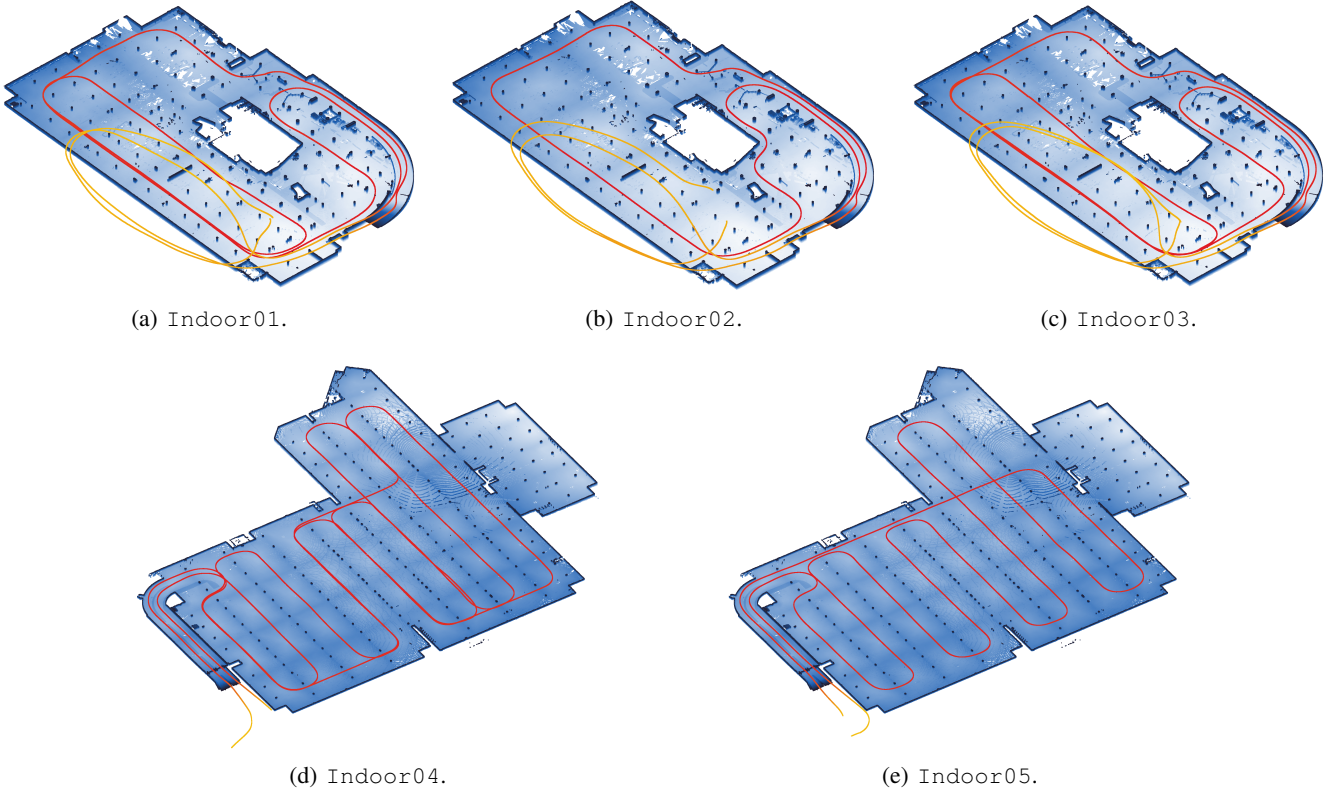


Fig. 11: Indoor trajectories. Segments are colored according to their height, with the **yellow** portion recorded outside the garage and the **red** portion recorded inside. The garage ceiling is rendered transparent to enhance visualization.



Fig. 12: OAK camera images under different lighting conditions.

computed as the root-mean-square error between the estimated and the actual relative motions over a fixed time interval. We split the analysis into translational error (*trans*) expressed in meters and rotational error (*rot*) expressed in degrees.

B. LiDAR Odometry

For LiDARs, we demonstrate the data validity using LiDAR odometry (LO) with the renowned Kiss-ICP algorithm [18]. This method has proven to deliver efficient and competitive state-of-the-art performance in odometry-based pose estimation, relying on LiDAR-only measurements.

We utilized point cloud data from both LiDARs across two different urban trajectories, resulting in two separate LO solutions: Velodyne-LO and Livox-LO. The obtained solutions in each trajectory were compared to the high-precision positioning reference solution to assess their accuracy.

Fig. 14 qualitatively demonstrates the performance of the estimated LO solutions for the Urban03 and Urban04 trajectories. The solutions are plotted in 2D along the east and north axes, with the starting point set at coordinates $(0, 0)$. The precise and detailed spatial information obtained from the LiDAR measurements results in trajectories that closely align with the reference. This demonstrates the ability the algorithm combined with LiDAR measurement to capture the dynamics for the entirety of both urban trajectories.

Although the 2D plots in Fig. 14 suggest that both LiDARs offer comparable LO performance, with Livox-LO showing slightly better alignment, TABLE IV presents further insights. The ATE statistics for both position and rotation indicate a noticeable difference between the two systems. This is likely influenced by the vertical resolution of the Velodyne LiDAR impacting the estimation of the vertical pose components.

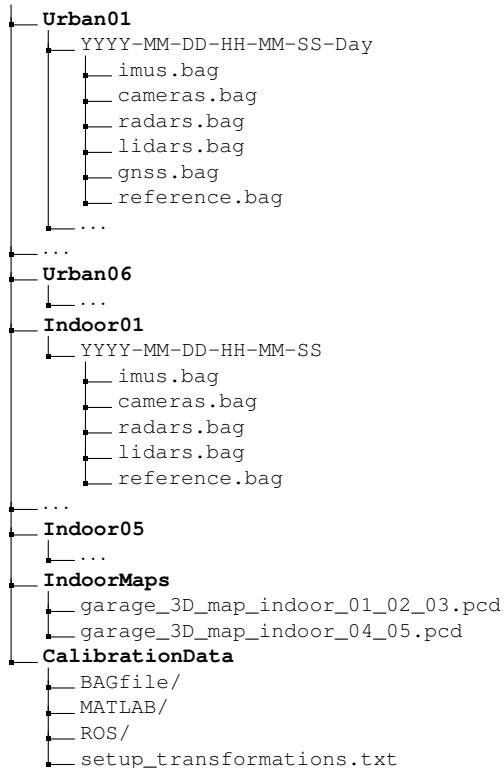


Fig. 13: Data organization.

TABLE IV: Performance statistics from the two LiDARs in both trajectories.

Sequence	Method	ATE		RPE	
		trans (m)	rot (°)	trans (m)	rot (°)
Urban03 (D)	Livox-LO	6.75	1.89	0.1114	0.2145
	Velodyne-LO	65.40	13.49	0.1425	0.1830
Urban04 (D)	Livox-LO	23.61	2.79	0.1219	0.1136
	Velodyne-LO	109.16	22.41	0.2033	0.1343

Regarding RPE, Livox-LO shows better translational accuracy, while the rotational performance varies between the two systems. Researchers are encouraged to further investigate the advantages of these cost-effective LiDAR sensors, as well as the challenges posed by their varying specifications across different scenarios.

C. Inertial Navigation System

We employed the standard inertial navigation system (INS) algorithm to demonstrate the validity of the IMU data [19]. The INS algorithm processes linear acceleration and angular velocity measurements from each IMU, generating a distinct INS solution. To mitigate the inherent drift in the INS, the algorithm is complemented by the forward speed from the vehicle's odometer and the non-holonomic constraint for vehicular motion [20]. Additionally, initial biases in IMU measurements were estimated and corrected using data from a stationary period at the start of each trajectory, except the high-end IMU, where such corrections were not necessary.

TABLE V: Performance statistics from all IMUs in both trajectories.

Trajectory	Method	ATE		RPE	
		trans (m)	rot (°)	trans (m)	rot (°)
Urban03 (D)	KVH	7.01	0.65	0.0044	0.0347
	Xsens	11.61	1.11	0.0049	0.0348
	Livox	9.31	1.16	0.0045	0.0349
	ZEDX-L	43.21	10.58	0.0171	0.0363
	ZEDX-R	42.59	7.34	0.0121	0.0354
Urban04 (D)	KVH	10.69	0.96	0.0034	0.0132
	Xsens	13.72	1.74	0.0045	0.0073
	Livox	19.35	1.87	0.0047	0.0124
	ZEDX-L	205.35	26.18	0.0567	0.0082
	ZEDX-R	175.61	22.71	0.0494	0.0066

Given that some IMUs exhibited significant drift, we limited the demonstration to 5-minute scenarios from the Urban03 and Urban04 trajectories. The performance of various IMUs across these scenarios is presented in the 2D plots of Fig. 15. As anticipated, the KVH1750 IMU closely aligned with the reference trajectory in both scenarios, and the commercial IMU inside the Xsens unit also presented robust performance. The Livox built-in IMU demonstrated strong performance in both scenarios. In contrast, the IMUs integrated within the ZED X cameras showed the least accurate performance, with considerable drift observed over extended periods.

TABLE V provides a quantitative analysis of the IMU performance, with the KVH1750 IMU exhibiting superior ATE statistics in both translation and rotation, followed by the Livox and Xsens IMUs. The IMUs integrated into the cameras, however, clearly faced notable challenges resulting in significantly higher ATE values. The RPE statistics reflect a similar trend, with the KVH IMU showing the best translation performance and the camera IMUs recording the highest RPEs.

These results highlight the diverse range of IMU measurements our system offers, accommodating various levels of IMU quality from low-cost, built-in camera IMUs to the high-end tactical-grade KVH1750 IMU. This diversity allows researchers and practitioners to explore and investigate the potential and limitations of different IMU grades.

D. Monocular Visual Odometry

To validate some of the camera systems available in this dataset, we integrating cameras and inertial systems to perform monocular visual odometry (MVO) on land vehicles [21], [22]. The method used relies on Shi-Tomasi features, provided by OpenCV's *goodFeaturesToTrack* and pyramidal optical flow to track features, thus performing essential matrix estimation and recovering motion without having to perform the time-consuming feature matching operation. Fig. 16 shows the tracked features across the three cameras chosen for this demonstration.

Fig. 17 shows samples from the MVO solutions, with translation scaled by the speed acquired from the odometer. Camera features are affected by moving objects in the scene; thus, the right camera consistently performs better than the left, where cars commonly pass in the opposing direction.

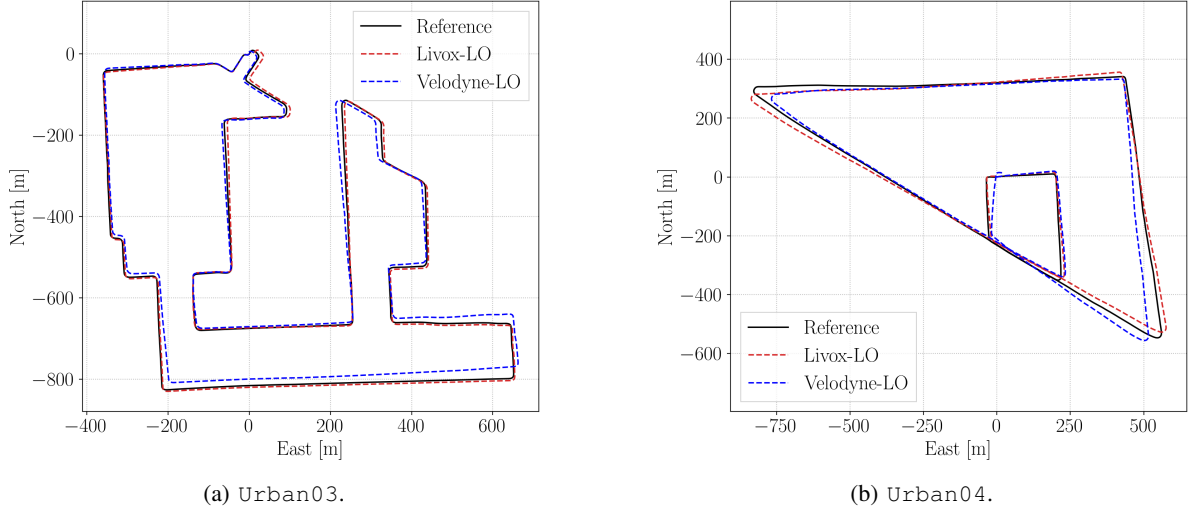


Fig. 14: LO performance from the two LiDARs.

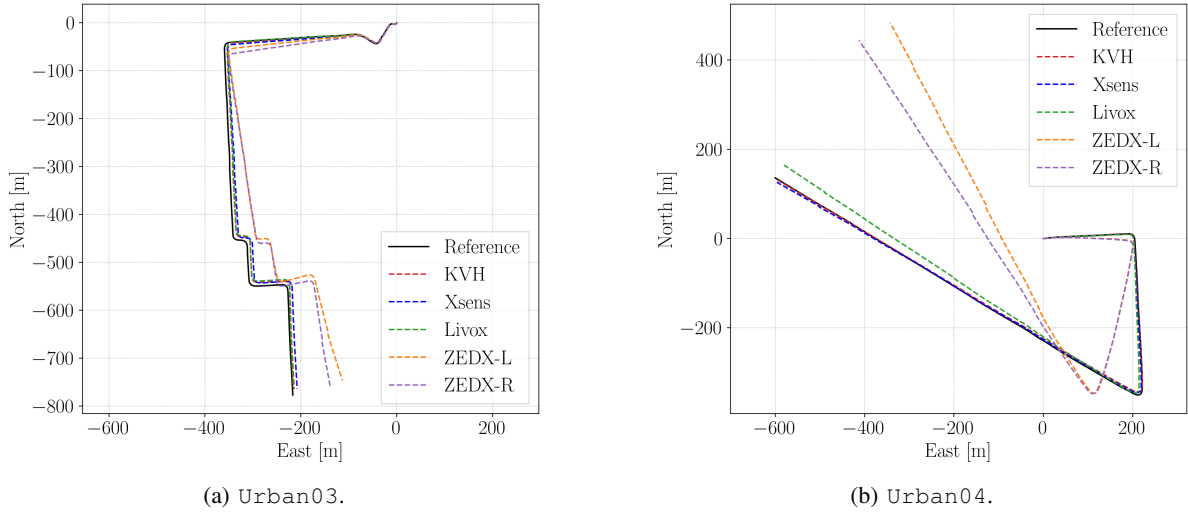


Fig. 15: INS performance across different IMUs.

TABLE VI: Performance statistics from different cameras in both trajectories.

Trajectory	Method	ATE		RPE	
		trans (m)	rot ($^{\circ}$)	trans (m)	rot ($^{\circ}$)
Urban03 (D)	OAK-MVO	39.74	10.63	0.0726	0.1087
	ZEDX-L-MVO	108.63	9.34	0.1201	0.1341
	ZEDX-R-MVO	82.00	11.84	0.1259	0.1295
Urban04 (D)	OAK-MVO	91.83	4.74	0.1309	0.0875
	ZEDX-L-MVO	113.06	9.14	0.1921	0.1343
	ZEDX-R-MVO	35.37	5.60	0.1651	0.1420

TABLE VI shows the MVO performance across the selected cameras. Consistent with evidence in the computer vision literature, standalone cameras cannot provide long-term positioning solutions. However, we believe that by providing data from a multi-view platform, our dataset will contribute to recent multi-modal data fusion trends in computer vision.

E. Stereo Visual Simultaneous Localization and Mapping

We also demonstrate the applicability of the cameras for stereo visual simultaneous localization and mapping (VS-LAM). In this application, we are interested in localizing the camera while building a map of the environment [23]. The process begins with a map initialization, where a 3D map is generated from a pair of stereo images, with the left image stored as the first keyframe and 3D points derived from the disparity map.

In the subsequent stage, i.e., tracking, the camera's pose is estimated by matching features in the left image to the last keyframe and refined by tracking the disparity, ensuring accuracy in the estimated trajectory. Next, new map points are added if the current left image is identified as a keyframe, with bundle adjustment minimizing reprojection errors by refining both the camera's pose and 3D points. The final stage ensures long-term map consistency by detecting and optimizing loop closures, refining the camera's pose and 3D map to correct any drift.

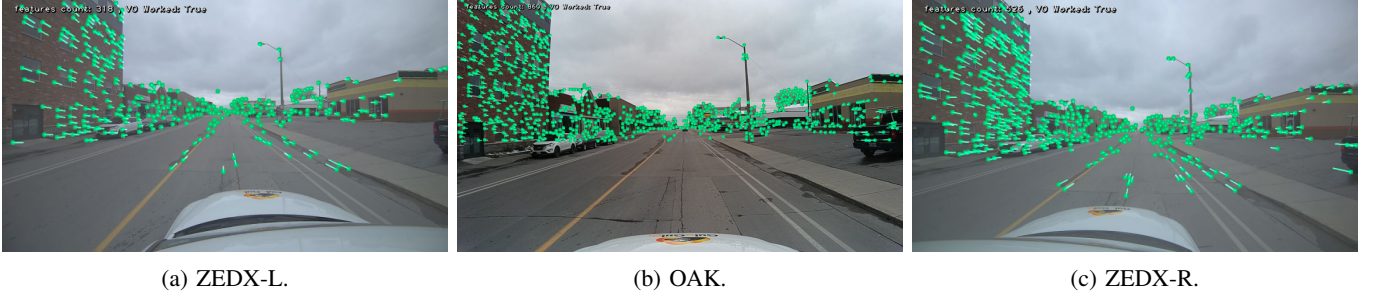


Fig. 16: Shi-Tomasi Features tracked across the three selected cameras.

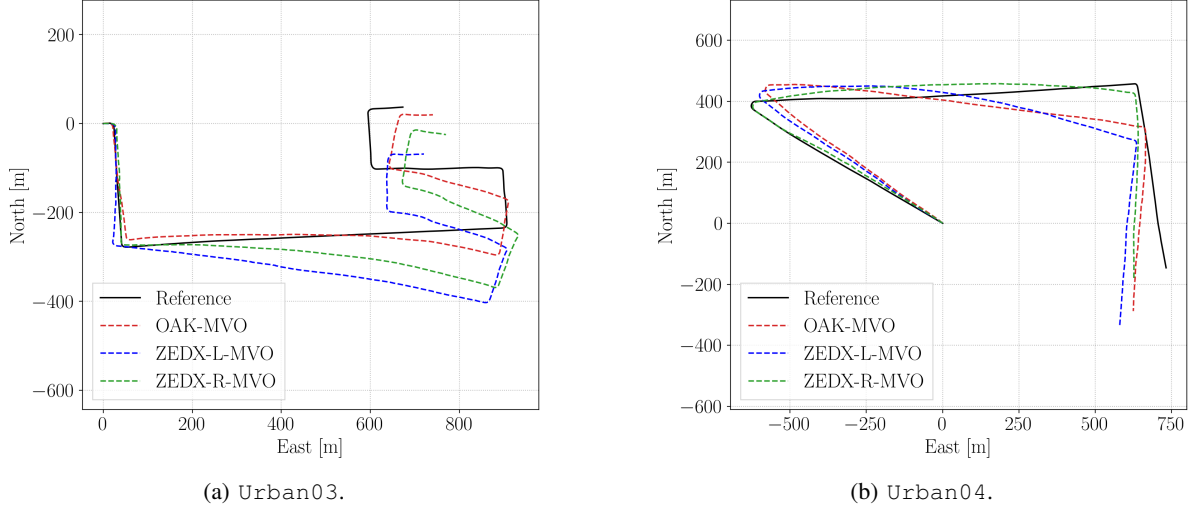


Fig. 17: MVO performance across different cameras.

Fig. 18 presents the results obtained with the ZED X (left) stereo camera. It can be seen that the method captures the vehicle's dynamics, albeit with some scale error. The stereo camera has a wide field of view and a short baseline, which can affect the accuracy of depth estimation and, consequently, the scale of the estimated poses. The blue dots represent the detections included in the map. This scenario, along with all indoor trajectories, offers many research opportunities, especially since the ground truth map of the garage is provided.

TABLE VII presents the evaluation metrics for both the estimated and optimized trajectories. The optimization process noticeably improved the ATE in translation, reducing it from 6.56 meters to 3.83 meters. However, this optimization negatively impacted the rotation metrics, which could be attributed to the lack of loops in the tested scenario. Overall, the results highlight the potential of the cameras in the platform for application to various advanced methods. Users can create stereo rigs using the available cameras and take advantage of longer baselines.

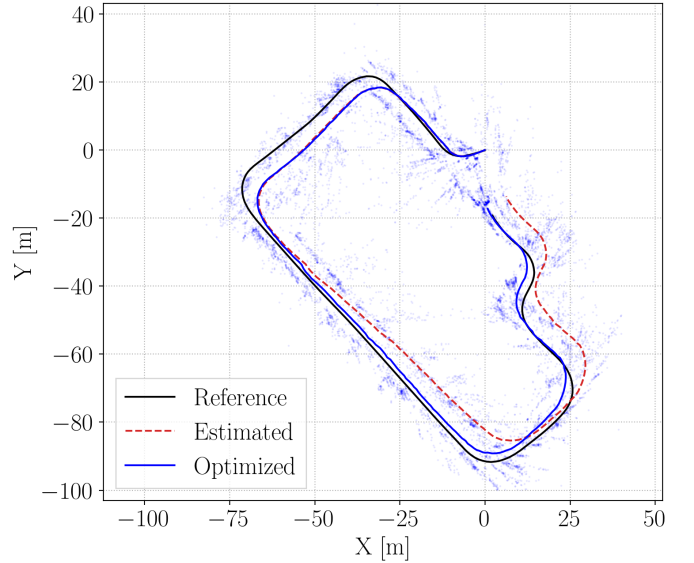


Fig. 18: Performance of Stereo VSLAM in Indoor02.

F. RADAR Odometry and Map Registration

The validity of the RADAR data from the four Smartmicro RADARs is demonstrated through the implementation of two RADAR-based localization methods applied to an indoor trajectory: RADAR-Inertial Odometry (RIO) and a RADAR-to-map registration (RMR) positioning solution. The RIO method

leverages the Doppler velocities and azimuths of targets returned by the ESR to estimate the instantaneous forward velocity of the vehicle following the procedure outlined in [24], which is then used as forward speed updates in an INS mechanization as in [25]. The RMR method employs

TABLE VII: VSLAM performance statistics in indoor settings using the ZED X (Left) stereo camera.

Trajectory	Method	ATE		RPE	
		trans (m)	rot ($^{\circ}$)	trans (m)	rot ($^{\circ}$)
Indoor02	Estimated	6.56	2.31	0.1534	0.3103
	Optimized	3.83	2.82	0.1586	0.6897

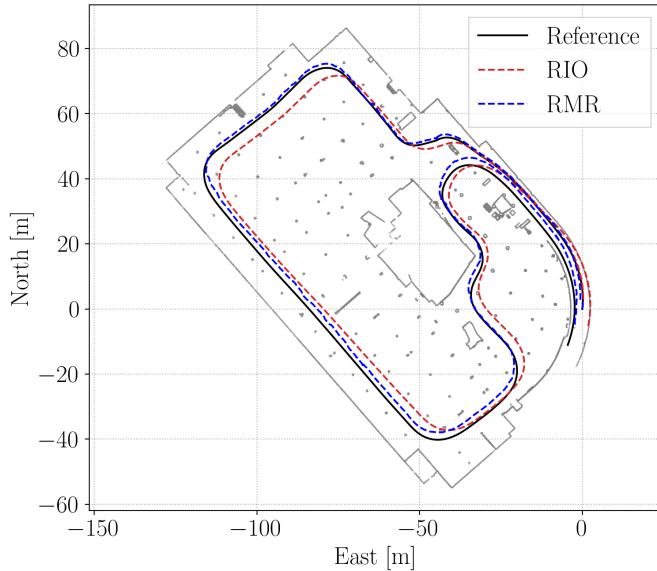


Fig. 19: RIO vs. RMR performance in Indoor02 Trajectory.

the iterative closest point (ICP) algorithm to register RADAR scans to a map of the environment for positioning corrections, following methods presented in [25].

Fig. 19 shows the performance of both the RIO and the RMR solutions in an indoor parking garage, compared to the ground truth solution. A quantitative analysis of the solutions is provided in TABLE VIII. RIO, as a dead reckoning solution, drifts throughout the course of the 2.7-minute trajectory, while RMR maintains bounded positioning errors throughout the entire experiment.

Localization using automotive RADARs remains a challenging task due to their comparatively low resolution and high noise and clutter levels. However, these results demonstrate the promise of automotive RADAR as an aiding sensor in automotive localization. The dataset facilitates research into the emerging possibilities and challenges relating to automotive RADAR as a localization sensor.

TABLE VIII: RADAR performance statistics in indoor settings.

Trajectory	Method	ATE		RPE	
		trans (m)	rot ($^{\circ}$)	trans (m)	rot ($^{\circ}$)
Indoor02	RIO	3.79	2.51	0.0170	0.0263
	RMR	1.89	3.37	0.1065	0.3650

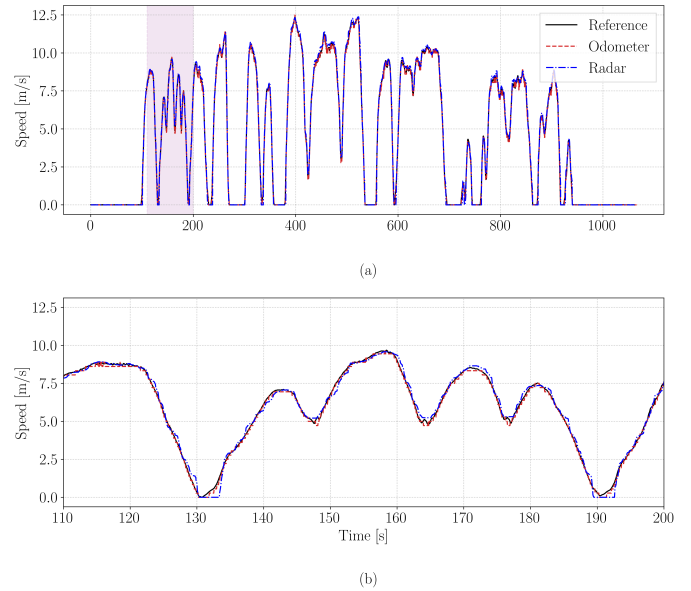


Fig. 20: Vehicle's forward speed comparison.

G. Forward Speed using RADAR

The RADAR mounted on the vehicle's front bumper can be used to estimate the vehicle's forward speed. As the sensor faces the ground at an angle, it measures the relative speed between the vehicle and the ground. Since the ground is always available and stationary, it is possible to infer the vehicle's forward speed by knowing the sensor's mounting angle.

The challenge lies in the accurate computation of the mounting angle, as vehicles have different shapes and mounting positions. To solve this problem, some researchers proposed a deep-learning-based method to calibrate the mounting angle and denoise the signal [26]. The system is based on a denoising autoencoder and is trained using a reference system.

Fig. 20 demonstrates such an approach. The blue dashed line represents the results of the denoising autoencoder, which was trained using the reference system, i.e., Novatel PwrPak7-E1 + KVH1750 IMU. We compare the RADAR-based estimation to the reference system and the odometer. As seen in the highlighted area magnified in Fig. 20(b), the model performs well and captures most of the dynamics.

The RADAR-based estimation obtained a root-mean-squared error of 0.24 m/s when compared to the reference system, while the odometer-based estimation achieved 0.11 m/s. Practitioners can implement different methods or strategies to improve the results and generate a reliable and redundant source of forward speed measurement.

VII. CONCLUSION

This paper introduces the NavINST dataset, a comprehensive collection of land vehicle trajectories recorded under various lighting conditions and across diverse urban and indoor environments. Designed to support the research community, our open-source dataset is fully integrated with ROS, offering both accessibility and ease of use. The primary objective of this dataset is to contribute to the advancement of navigation and positioning research, particularly in the development

and validation of robust algorithms for future commercial autonomous vehicles. However, we also encourage researchers to explore and adapt this dataset for a wide range of other research applications beyond autonomous navigation.

The dataset provides a plethora of sensors, including multiple-grade IMUs, GNSS, monocular and stereo cameras, mechanical and solid-state LiDARs, automotive RADARs, and onboard vehicle measurements. We demonstrate the validity and effectiveness of our sensor data through comprehensive demonstrations employing various navigation algorithms. These demonstrations underscore the potential of the dataset to facilitate a vast range of navigation-related research endeavours. This project is an ongoing effort, and future work will focus on further enriching the NavINST dataset. We plan to investigate the inclusion of additional sensors, explore new environments, and expand the dataset's applicability to a broader range of scenarios. These enhancements will be guided by feedback from the research community, ensuring that the dataset continues to evolve to better support navigation and positioning research.

ACKNOWLEDGMENT

This research is supported by grants from the Natural Sciences and Engineering Research Council of Canada (NSERC) under grant numbers RGPIN-2020-03900 and ALLRP-560898-20. The authors also thank Tristan Redish and Marc Adam for their invaluable support during the execution of this project and for coordinating work between different technical departments. In addition, we extend our gratitude to past members of the NavINST Lab, whose foundational experiments and insightful discussions have significantly contributed to the evolution of this work. Finally, we thank Micro Engineering Tech Inc. (METI) for their technical support and for preparing and providing the 3D maps of the indoor garages.

REFERENCES

- [1] J. Lutin, "Not if, but when: autonomous driving and the future of transit," *Journal of Public transportation*, vol. 21, pp. 92–103, 2018.
- [2] T. G. Reid, S. E. Houts, R. Cammarata, G. Mills, S. Agarwal, A. Vora, and G. Pandey, "Localization requirements for autonomous vehicles," *SAE International Journal of Connected and Automated Vehicles*, vol. 2, no. 12-02-03-0012, pp. 173–190, 2019.
- [3] A. Geiger, P. Lenz, C. Stiller, and R. Urtasun, "Vision meets robotics: The KITTI dataset," *The International Journal of Robotics Research*, vol. 32, no. 11, pp. 1231–1237, Sep. 2013.
- [4] W. Maddern, G. Pascoe, C. Linegar, and P. Newman, "1 year, 1000 km: The Oxford RobotCar dataset," *The International Journal of Robotics Research*, vol. 36, no. 1, pp. 3–15, Jan. 2017.
- [5] J. Jeong, Y. Cho, Y.-S. Shin, H. Roh, and A. Kim, "Complex Urban LiDAR Data Set," in *2018 IEEE international conference on robotics and automation (ICRA)*. IEEE, 2018, pp. 6344–6351.
- [6] G. Kim, Y. S. Park, Y. Cho, J. Jeong, and A. Kim, "MulRan: Multimodal Range Dataset for Urban Place Recognition," in *2020 IEEE International Conference on Robotics and Automation (ICRA)*. Paris, France: IEEE, May 2020, pp. 6246–6253.
- [7] L.-T. Hsu, F. Huang, H.-F. Ng, G. Zhang, Y. Zhong, X. Bai, and W. Wen, "Hong Kong UrbanNav: An Open-Source Multisensory Dataset for Benchmarking Urban Navigation Algorithms," *NAVIGATION: Journal of the Institute of Navigation*, vol. 70, no. 4, p. navi.602, 2023.
- [8] K. Burnett, D. J. Yoon, Y. Wu, A. Z. Li, H. Zhang, S. Lu, J. Qian, W.-K. Tseng, A. Lambert, K. Y. Leung *et al.*, "Boreas: A Multi-Season Autonomous Driving Dataset," *The International Journal of Robotics Research*, vol. 42, no. 1-2, pp. 33–42, 2023.
- [9] D. Barnes, M. Gadd, P. Murcutt, P. Newman, and I. Posner, "The Oxford Radar RobotCar Dataset: A Radar Extension to the Oxford RobotCar Dataset," in *2020 IEEE international conference on robotics and automation (ICRA)*. IEEE, 2020, pp. 6433–6438.
- [10] M. Choi, S. Yang, S. Han, Y. Lee, M. Lee, K. H. Choi, and K.-S. Kim, "MSC-RAD4R: ROS-Based Automotive Dataset With 4D Radar," *IEEE Robotics and Automation Letters*, vol. 8, no. 11, pp. 7194–7201, Nov. 2023.
- [11] D.-H. Paek, S.-H. Kong, and K. T. Wijaya, "K-Radar: 4D Radar Object Detection for Autonomous Driving in Various Weather Conditions," Nov. 2023.
- [12] J.-L. Déziel, P. Meriaux, F. Tremblay, D. Lessard, D. Plourde, J. Stanguennec, P. Goulet, and P. Olivier, "PixSet : An Opportunity for 3D Computer Vision to Go Beyond Point Clouds With a Full-Waveform LiDAR Dataset," in *2021 IEEE international intelligent transportation systems conference (itsc)*. IEEE, 2021, pp. 2987–2993.
- [13] P.-C. Kung, C.-C. Wang, and W.-C. Lin, "A normal distribution transform-based radar odometry designed for scanning and automotive radars," in *2021 IEEE International Conference on Robotics and Automation (ICRA)*, 2021, pp. 14417–14423.
- [14] M. Quigley, K. Conley, B. Gerkey, J. Faust, T. Foote, J. Leibs, R. Wheeler, A. Y. Ng *et al.*, "ROS: an open-source robot operating system," in *ICRA workshop on open source software*, vol. 3, no. 3.2. Kobe, Japan, 2009, p. 5.
- [15] R. Martins, D. Raposo, R. Lopes, P. Rito, and S. Sargento, "Time synchronization in V2X communications," in *2024 IEEE Vehicular Networking Conference (VNC)*. IEEE, 2024, pp. 25–32.
- [16] A. Pirti, "Evaluating the accuracy of post-processed kinematic (ppk) positioning technique," *Geodesy and Cartography*, vol. 47, pp. 66–70, 2021.
- [17] E. Mounier, M. Elhabiby, M. Korenberg, and A. Noureldin, "LiDAR-based multi-sensor fusion with 3D digital maps for high-precision positioning," *IEEE Internet of Things Journal*, pp. 1–1, 2024.
- [18] I. Vizzo, T. Guadagnino, B. Mersch, L. Wiesmann, J. Behley, and C. Stachniss, "Kiss-icp: In defense of point-to-point icp-simple, accurate, and robust registration if done the right way," *IEEE Robotics and Automation Letters*, vol. 8, no. 2, pp. 1029–1036, 2023.
- [19] A. Noureldin, T. B. Karamat, and J. Georgy, *Fundamentals of inertial navigation, satellite-based positioning and their integration*. Springer Science & Business Media, 2012.
- [20] E. Mounier, M. J. Korenberg, and A. Noureldin, "Online motion sensors error modelling for robust navigation using fast orthogonal search," in *2022 5th International Conference on Communications, Signal Processing, and their Applications (ICCSIPA)*. IEEE, 2022, pp. 1–6.
- [21] S. I. K. Abdelaziz, A. Noureldin, and G. Fotopoulos, "Low-cost indoor vision-based navigation for mobile robots," in *Proceedings of the 33rd International Technical Meeting of the Satellite Division of The Institute of Navigation (ION GNSS+ 2020)*, 2020, pp. 2560–2568.
- [22] S. I. K. Abdelaziz, H. Y. Elghamrawy, A. M. Noureldin, and G. Fotopoulos, "Body-centered dynamically-tuned error-state extended kalman filter for visual inertial odometry in GNSS-denied environments," *IEEE Access*, vol. 12, pp. 15 997–16 008, 2024.
- [23] R. Mur-Artal and J. D. Tardós, "ORB-SLAM2: An open-source SLAM system for monocular, stereo, and RGB-D cameras," *IEEE transactions on robotics*, vol. 33, no. 5, pp. 1255–1262, 2017.
- [24] D. Kellner, M. Barjenbruch, J. Klappstein, J. Dickmann, and K. Dietmayer, "Instantaneous ego-motion estimation using doppler radar," in *Proceedings of the 16th International IEEE Annual Conference on Intelligent Transportation Systems*, October 2013.
- [25] E. Dawson, "Integrated remote sensing and map registration system for high-precision positioning in covered parking garages," in *Proceedings of the 36th International Technical Meeting of the Satellite Division of The Institute of Navigation (ION GNSS+ 2023)*, 2023, pp. 1633–1643.
- [26] P. R. M. de Araujo, M. Elhabiby, S. Givigi, and A. Noureldin, "A novel method for land vehicle positioning: Invariant kalman filters and deep-learning-based radar speed estimation," *IEEE Transactions on Intelligent Vehicles*, vol. 8, no. 9, pp. 4275–4286, 2023.